

Supplementary Materials: Quantifying impacts of aerosol mixing state on nucleation-scavenging of black carbon aerosol particles

1 Joseph Ching ^{1*}, Matthew West ² and Nicole Riemer ³

2 Overview

3 This supplementary material document contains six figures to provide additional information
4 for understanding the nucleation scavenging phenomenon of BC-containing particles. We also
5 present a short derivation how mass-based and number-based scavenging fractions are related.

6 Figures S1 and S2 show the number-based scavenging fraction of BC-containing particles, which
7 correspond to the mass-based scavenging fraction shown in Figure 3 and 4 in the main text.

8 Figure S3 shows the BC mass distributions for the BC-containing particles undergoing
9 nucleation-scavenging (blue) and for all BC-containing particles (red), averaged over all 384 aerosol
10 populations. The blue distributions show the average nucleation-scavenged BC mass concentration
11 distribution for the four different environmental supersaturations, and the red distributions show the
12 total BC mass concentration distributions, both as functions of BC core diameter. The size-resolved
13 nucleation-scavenged BC mass fractions as shown in Figure 3 in the main manuscript are hence
14 obtained by dividing the values of the blue curves by the values of the red curves for each BC core
15 diameter. For the larger BC core diameters, there is little difference between red and blue curves,
16 indicating a nucleation-scavenged BC mass fraction of nearly 1. At smaller sizes, the red and blue
17 lines are further apart from each other, indicating a nucleation-scavenged BC mass fraction smaller
18 than 1. The fraction increases for increasing BC core diameters, but not necessarily monotonically.

19 Figure S4 presents mass-based BC scavenging fraction errors. The figure compares the case for
20 size-resolved composition averaging (blue circles) with the case when composition averaging was
21 performed for the entire population (orange filled circles). The general dependence on χ remained
22 the same as in Figure 7 in the main manuscript, but the magnitude of the errors decreased. For
23 example, the maximum error using the size-resolved averaging (blue circles) was 1063% and 273% at
24 $s_{\text{env}} = 0.1\%$ and 0.6% , respectively; while the corresponding maximum errors for averaging over the
25 whole distribution (orange filled circles) were 2668% and 399%, respectively.

Figures S5 and S6 show the number-based total BC scavenging fraction, and the corresponding
errors when assuming internal mixture, respectively, as a function of mixing state metric χ .
Analogous to equation (3) in the main manuscript, the number-based nucleation scavenging fraction
is defined at supersaturation s_{env} as

$$f_{\text{BC}}^N(s_{\text{env}}) = \frac{n_{\text{ns,BC}}(s_{\text{env}})}{n_{\text{BC}}}, \quad (1)$$

26 where $n_{\text{ns,BC}}(s_{\text{env}})$ and n_{BC} are number concentration of BC-containing CCN at supersaturation s_{env} ,
27 and total number concentration of BC-containing particles, respectively.

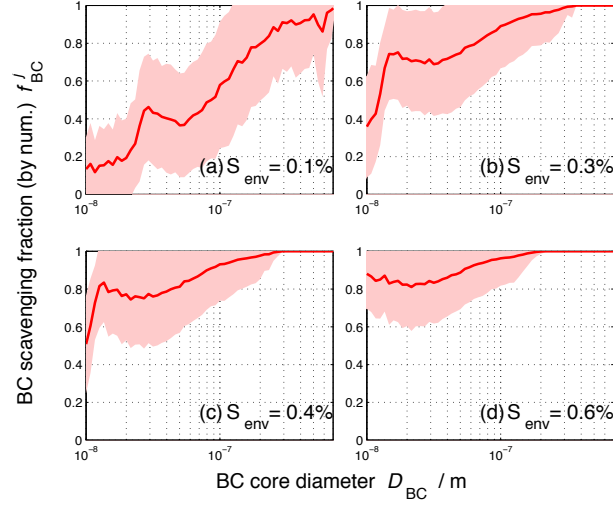


Figure S1. The size-resolved nucleation-scavenged BC number fraction, as a function of black carbon core diameter, D_{BC} , at four selected supersaturation values: 0.1%, 0.3%, 0.4%, and 0.6%. The solid line represents the average over the 384 populations, and the color shading indicates one standard deviation.

28 Relationship of number-based and mass-based nucleation-scavenged BC mass fractions

Let us define the mass concentration of BC-containing particles with BC core diameter between D_{BC} and $D_{BC} + dD_{BC}$, and critical supersaturation between s and $s + ds$ as $m_{ns,BC}(D_{BC}, s)$. The number concentration of BC-containing particles between D_{BC} and $D_{BC} + dD_{BC}$, and critical supersaturation between s and $s + ds$ is $n_{ns,BC}(D_{BC}, s)$. Then, the mass-based nucleation-scavenging fraction $f_{BC}(D_{BC}, s_{env})$ for particles in size range D_{BC} and $D_{BC} + dD_{BC}$ and an environmental supersaturation s_{env} is given by

$$f_{BC}(D_{BC}, s_{env}) = \frac{\int_0^{s_{env}} m_{ns,BC}(D_{BC}, s) ds}{\int_0^{\infty} m_{ns,BC}(D_{BC}, s) ds}. \quad (2)$$

Similarly, we can define the number-based nucleation-scavenging fraction $f_{BC}^N(D_{BC}, s_{env})$ for particles in size range D_{BC} and $D_{BC} + dD_{BC}$ and an environmental supersaturation s_{env} as

$$f_{BC}^N(D_{BC}, s_{env}) = \frac{\int_0^{s_{env}} n_{ns,BC}(D_{BC}, s) ds}{\int_0^{\infty} n_{ns,BC}(D_{BC}, s) ds} \quad (3)$$

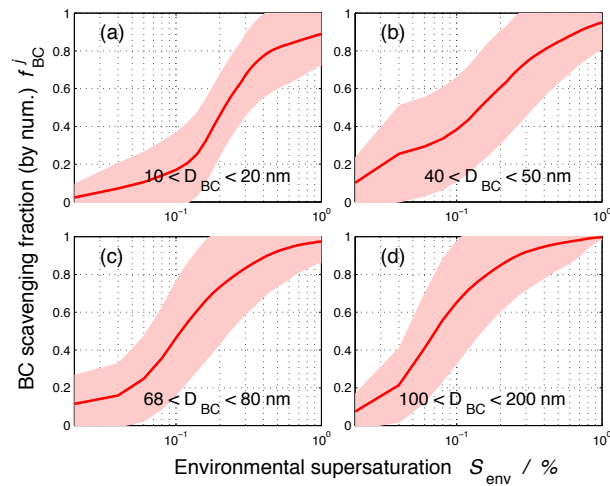


Figure S2. The nucleation-scavenged BC number fraction for selected size ranges as a function of supersaturation. The solid line represents the average over the 384 populations, and the color shading indicates one standard deviation.

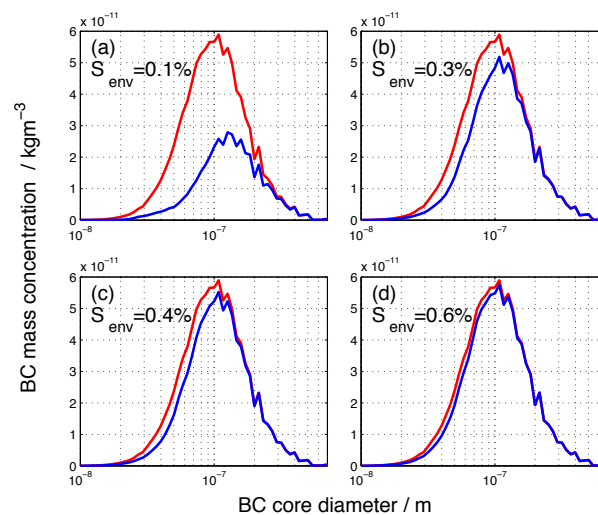


Figure S3. BC mass size distributions as a function of BC core diameter for the nucleation-scavenged BC-containing particles (blue), and for all BC-containing particles (red) for selected supersaturations. The distributions are the average over all 384 populations.

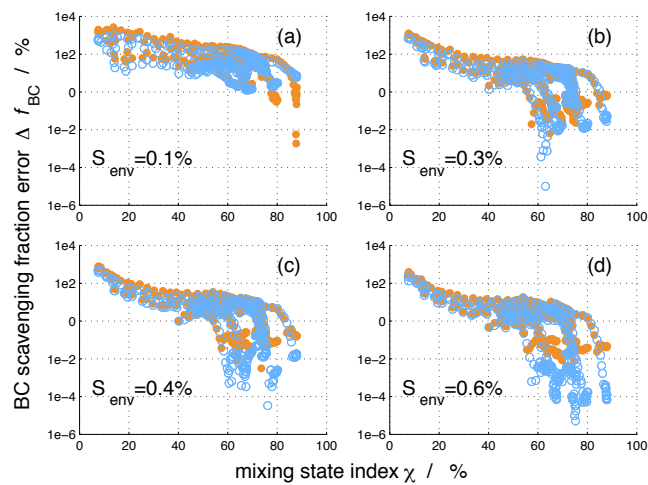


Figure S4. The absolute value of the error in black carbon nucleation-scavenged mass fraction, $|\Delta f_{BC}|$, for the 384 aerosol populations calculated with size-resolved composition-averaged aerosol populations (blue circles) and for composition-averaging of the entire population (orange filled circles), at four selected supersaturation values: 0.1%, 0.3%, 0.4%, and 0.6% as a function of mixing state index χ .

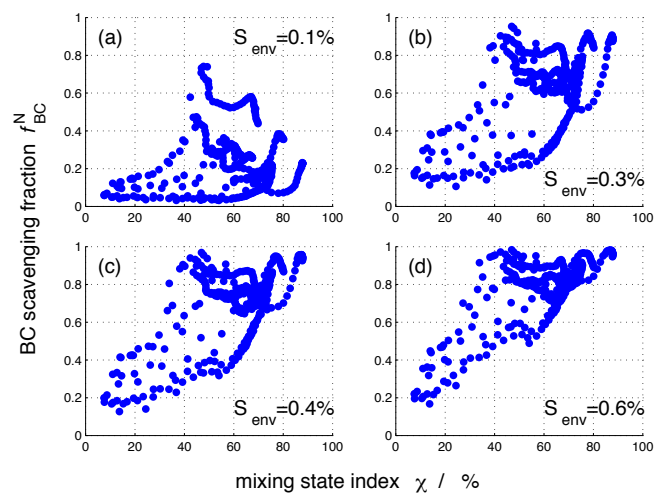


Figure S5. The total nucleation-scavenged BC number fraction, f_{BC}^N , for the 384 aerosol populations as a function of aerosol mixing state index χ , at four selected supersaturation values: 0.1%, 0.3%, 0.4%, and 0.6%.

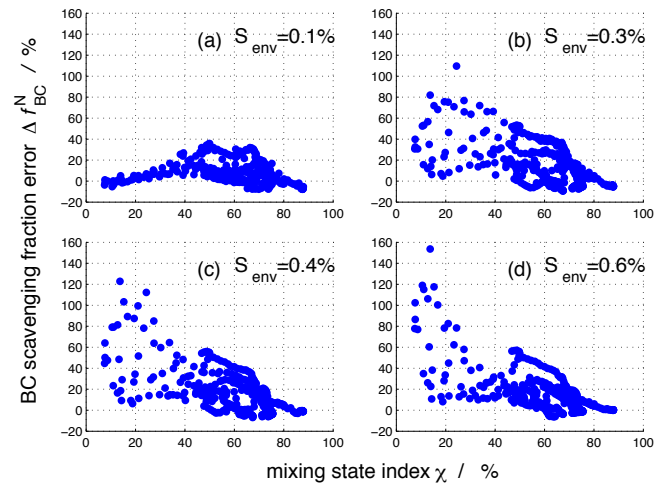


Figure S6. The error in total nucleation-scavenged BC number fraction, Δf_{BC}^N , for the 384 aerosol populations as a function of aerosol mixing state index χ , at four selected supersaturation values: 0.1%, 0.3%, 0.4%, and 0.6%.

Equations (2) and (3) are equivalent as can be seen from the following:

$$\begin{aligned}
 f_{BC}(D_{BC}, s_{env}) &= \frac{\int_0^{s_{env}} m_{ns,BC}(D_{BC}, s) ds}{\int_0^{\infty} m_{ns,BC}(D_{BC}, s) ds} \\
 &= \frac{\int_0^{s_{env}} \frac{\pi}{6} D_{BC}^3 \rho_{BC} n_{ns,BC}(D_{BC}, s) ds}{\int_0^{\infty} \frac{\pi}{6} D_{BC}^3 \rho_{BC} n_{ns,BC}(D_{BC}, s) ds} \\
 &= \frac{D_{BC}^3 \int_0^{s_{env}} n_{ns,BC}(D_{BC}, s) ds}{D_{BC}^3 \int_0^{\infty} n_{ns,BC}(D_{BC}, s) ds} \\
 &= \frac{\int_0^{s_{env}} n_{ns,BC}(D_{BC}, s) ds}{\int_0^{\infty} n_{ns,BC}(D_{BC}, s) ds} \\
 &= f_{BC}^N(D_{BC}, s_{env}).
 \end{aligned} \tag{4}$$

Let us further define the total nucleation-scavenged BC mass fraction at a chosen environmental supersaturation s_{env} as

$$f_{BC}(s_{env}) = \frac{\int_0^{s_{env}} \int_0^{\infty} m_{ns,BC}(D_{BC}, s) dD_{BC} ds}{\int_0^{\infty} \int_0^{\infty} m_{ns,BC}(D_{BC}, s) dD_{BC} ds} \tag{5}$$

The total nucleation-scavenged BC number fraction at s_{env} is

$$f_{BC}^N(s_{env}) = \frac{\int_0^{s_{env}} \int_0^{\infty} n_{ns,BC}(D_{BC}, s) dD_{BC} ds}{\int_0^{\infty} \int_0^{\infty} n_{ns,BC}(D_{BC}, s) dD_{BC} ds}. \tag{6}$$

Equations (5) and (6) are not equivalent as can be shown as follows:

$$\begin{aligned}
 f_{\text{BC}}(s_{\text{env}}) &= \frac{\int_0^{s_{\text{env}}} \int_0^{\infty} m_{\text{ns,BC}}(D_{\text{BC}}, s) \, dD_{\text{BC}} \, ds}{\int_0^{\infty} \int_0^{\infty} m_{\text{ns,BC}}(D_{\text{BC}}, s) \, dD_{\text{BC}} \, ds} \\
 &= \frac{\int_0^{s_{\text{env}}} \int_0^{\infty} \frac{\pi}{6} D_{\text{BC}}^3 \rho_{\text{BC}} n_{\text{ns,BC}}(D_{\text{BC}}, s) \, dD_{\text{BC}} \, ds}{\int_0^{\infty} \int_0^{\infty} \frac{\pi}{6} D_{\text{BC}}^3 \rho_{\text{BC}} n_{\text{ns,BC}}(D_{\text{BC}}, s) \, dD_{\text{BC}} \, ds} \\
 &= \frac{\int_0^{s_{\text{env}}} \int_0^{\infty} D_{\text{BC}}^3 n_{\text{ns,BC}}(D_{\text{BC}}, s) \, dD_{\text{BC}} \, ds}{\int_0^{\infty} \int_0^{\infty} D_{\text{BC}}^3 n_{\text{ns,BC}}(D_{\text{BC}}, s) \, dD_{\text{BC}} \, ds}. \tag{7}
 \end{aligned}$$